Advances in Welding Technology & Science
ASM, Metals Park, Ohio, U.S.A.
1987 225-229

PREDICTION OF MICROSTRUCTURE OF THE FUSION ZONE OF MULTICOMPONENT STEEL WELD DEPOSITS

H.K.D.H. Bhadeshia
University of Cambridge
Cambridge, U.K.

Lars-Erik Svensson, B. Gretoft
ESAB AB
Gothenburg, Sweden

ABSTRACT

A model based on phase transformation theory, has been developed to allow the prediction of steel weld metal microstructures. It requires the input of just chemical composition and welding conditions; this facilitates the calculation of the appropriate part of the phase diagram (for steels containing C, Mn, Si, Ni, Cr, Mo and V in any combination), needed to define the relevant paraequilibrium tie-lines for detailed kinetic analysis. TTT and CCT curves are also computed, together with various transformation start and finish temperatures. These data in turn lead to the estimation of the volume fractions of allotriomorphic ferrite, Widdmanstätten ferrite and acicular ferrite. The theory is found to be in good agreement with experimental results.

WELDING is a complex metallurgical process involving many variables; in this work we present a recent model (1-5) for the calculation of the primary microstructure of low-alloy steel welds. The model has been shown to be capable of predicting the primary microstructure of Fe-Mn-Si-C and Fe-Mn-Si-Ni-C manual-metal-arc (MMA) welds as a function of heat input and chemical composition (1-5). Here we demonstrate its application by analysing quantitatively, published data (6) on the effect of relatively large variations in Si and Mn concentrations, on the primary microstructure of MMA welds.

THEORY FOR THE PREDICTION OF THE MICROSTRUCTURE

In low-alloy steel welds, solidification begins with the epitaxial nucleation of δ-ferrite at the fusion boundary. The melt then solidifies by the cellular growth of δ (7) which in turn transforms into a columnar-austenite (γ) grain structure. The morphology of the γ grains can be represented as a honeycomb of hexagonal prisms, the side length of each prism being 'a' and the length of the prism being 'c' (3,8). The c-axes of these prisms are approximately parallel to the direction of maximum heat flow during solidification; if $\bar{L}_{tn}$ is the mean lineal intercept measured on a transverse section of the weld, in a direction normal to the major axes of the γ grains, then (3)

$$\bar{L}_{tn} = \pi a \cos(30^{o})/2, \qquad (1)$$

so that 'a' can be determined experimentally. The parameter 'c' is not needed for the microstructure calculations because c>>a so that any effect due to the ends of the hexagonal prisms can be neglected (1,3). On further cooling, at $T=T_h$, the γ begins to transform, to layers of allotriomorphic ferrite (α) which grow by a diffusional transformation mechanism, at the γ/γ boundaries. As the temperature falls, diffusional growth becomes more difficult and Widmanstätten ferrite (α_w) plates nucleate at the α/γ boundaries and grow into the γ by a displacive transformation mechanism (9-12), at a rate controlled approximately by the diffusion of C in the γ ahead of the plate tips (12). At the same time, acicular ferrite (α_a) nucleates on inclusions (and also by autocatalytic effects) within the γ grains and grows in the form of thin plates. As the M_s temperature is approached, the small amount of remaining austenite decomposes either into degenerate pearlite and/or mixtures of martensite and retained austenite; because the volume fraction of these phases is relatively small, they are called "microphases".

T_h is determined by using an additive reaction rule (1), the cooling curve and a computed Time-Temperature-Transformation (TTT) diagram for the alloy concerned (10). The TTT diagram consists of two 'C' curves, the upper one giving the time for the isothermal initiation of diffusional transformations such as α and pearlite, while the lower C curve represents the initiation times for displacive transformations such as α_w, α_a and bainite (10). The cross-over point of the two C curves is the temperature T_1 below

which displacive transformations are assumed to be kinetically favoured, so that the growth of α ceases and gives way to α_w and α_a formation. In the temperature range T_h-T_1, the α layers at the γ/γ boundaries are assumed to thicken by a paraequilibrium mechanism, at a rate controlled by the diffusion of carbon in the γ ahead of the moving α/γ interface. During isothermal transformation at a temperature T, the half thickness of each such layer is given by:

$$q = \alpha_1 t^{\frac{1}{2}} \qquad (2)$$

where α_1 is called the one-dimensional parabolic thickening rate constant, obtained by solving (see for example, ref. 11)

$$\{2(x^{\gamma\alpha}-\bar{x})/(x^{\gamma\alpha}-x^{\alpha\gamma})\}\{(\underline{D}/\pi)^{\frac{1}{2}}\}$$
$$= \alpha_1\{\exp[\alpha_1^2/(4\underline{D}/\pi)]\}\{1-\mathrm{erf}[\alpha_1/(2\underline{D}^{\frac{1}{2}})]\} \qquad (3)$$

and t is the time, defined to be zero when q=0. $x^{\alpha\gamma}$ and $x^{\gamma\alpha}$ are paraequilibrium carbon concentrations of α and of γ respectively, calculated as in Ref. 1. The diffusion coefficient D of carbon in γ is a sensitive function of the carbon concentration in austentite (x_γ) and since x_γ varies with distance ahead of the α/γ interface, a weighted average diffusion coefficient $\underline{D}$ is used in equation 2, and is defined as

$$\underline{D} = \int_{x^{\gamma\alpha}}^{\bar{x}} D\,dx/(\bar{x} - x^{\gamma\alpha}). \qquad (4)$$

Since the α grows anisothermally during cooling of the weld deposit, q is actually obtained by numerically integrating the function

$$q = \int_{t=0}^{t=t_1} 0.5\alpha_1\, t^{-0.5}\, dt \qquad (5)$$

where t_1 is the time taken for the weld deposit to cool from T_h to T_1. It should be noted that the parabolic rate constant is a function of time and temperature. The volume fraction v_α of α is then derived as a function of a and q:

$$v_\alpha = [4qC_3(a-2qC_3)/a^2] \qquad (6)$$

where $C_3 = \tan(30^\circ)$. A better fit is obtained by empirically correcting this to give a corrected volume fraction V^α (and this gives a corresponding corrected value of allotriomorph thickness q') where

$$V_\alpha = 2.04v_\alpha + 0.035, \qquad (7)$$

the calculated value thus being smaller than the actual value by a factor of ∿2, although the correlation between v_α and the actual volume fraction of α is typically found to be 0.95 (1).

At $T=T_1$, α_w formation begins, but the growth rate of α_w in welds is generally so high that growth ceases within a fraction of a second, and α_w formation can therefore be considered to occur isothermally at T_1. However, the volume fraction v_w of Widmanstätten ferrite in general correlates badly with its lengthening rate (G); impingement with acicular ferrite has to be taken into account. If the time available for unhindered α growth is t_2, then v_w is given by:

$$v_w = 3.34G(a-2q'C_3)t_2^2/a^2 \qquad (8)$$

G is calculated for $T=T_1$, by the method described in (12). In the absence of impingement with α_a, the time available for α_w to grow right across the γ grains is t_3, given by:

$$t_3 = 2[a\sin(60^\circ) - q']/G \qquad (9)$$

If t_3 is less than a critical time t_c, then α_w can grow without impingement with acicular ferrite and t_2 in Eq. (9) is set to equal t_3. On the other hand, if $t_c<t_3$ than α_w growth is terminated by impingement with α_a, t_2 is set equal to t_c. t_c is experimentally found to be 0.211s for welds containing inclusions which nucleate acicular ferrite; although t_c is not sensitive to oxygen concentration, it is recognised that it may vary, depending on the ability of inclusions to nucleate acicular ferrite. The microphase volume fraction v_m can also be estimated thermodynamically, so that:

$$v_a = 1 - V_\alpha - v_w - v_m \qquad (10)$$

where v_a is the volume fraction of α_a. It is usual to include the microphases in the v_w and v_a measurements, since v_m is generally small; hence, microphases are not measured or calculated separately in this work.

The high cooling rates associated with arc welding inevitably lead to solute segregation during solidification. The biggest effect of such segregation is to alter T_h (3); if solidification occurs with δ as the primary phase, then the partition coefficient k_i where i is the subscript identifying an alloy element) which gives the ratio of the mole fraction of i in δ to that in liquid is given at a temperature T by:

$$k_i = \exp\{\Delta^\circ G_i/(RT)\} \qquad (11)$$

where $\Delta^\circ G_i$ is the Gibbs free energy change per mole in transforming the pure i from δ to liquid, and R is the gas constant. It is assumed that the segregation arising during solidification is not influenced by subsequent diffusion during rapid cooling from the liquidus. The composition of regions which contain the lowest substitutional content is then given by $k_i\bar{x}_i$ where $\bar{x}_i$ is the average concentration of i and T is set to the melting point in Eq. (11), assumed to be 1520°C. Carbon is assumed uniform everywhere

since its activity gradients should rapidly be eliminated by diffusion during cooling. It follows that the compositions of the solute-depleted regions can be calculated, and these regions enhance ferrite nucleation. New TTT curves calculated for these solute-depleted regions can then be used to obtain better estimates of T_h. This procedure works well in calculating the microstructure of welds (3).

THE EFFECT OF Si ON WELD METAL MICROSTRUCTURE

From our knowledge of isothermal transformations in steels, it should at first sight be concluded that Si should enhance the formation of α in welds. Silicon is known to accelerate the nucleation and growth of ferrite (13). It should therefore increase V_α at the expense of, say, α_a. However, the development of microstructure during welding does not involve isothermal growth, and there are numerous other complicating and contradictory factors to be taken into account. It will become apparent later that information from isothermal experiments can be misleading in the context of weld deposits.

Evans (6) has reported quantitative microstructural measurements on a systematic series of Fe-Mn-Si-C alloys, in which the carbon concentration was kept approximately constant (0.065 wt.%). The aim of his work was to study the effect of silicon variations (~0.2-0.95 wt.%) at two levels of Mn (0.6, 1.4 wt.%). The compositions of the alloys concerned are given in Table 1. It is unfortunate that C varies significantly in these welds, because such variations are known to have a powerful effect on microstructure (1). This makes it difficult to isolate the effect of Si, since only welds 2 and 4, and welds 5 and 8 are comparable in terms of C and Mn.

Table 1 - Chemical compositions (wt.%) of welds studied by Evans (6). The austenite grain size 'a' is calculated as discussed in the text.

Weld	C	Mn	Si	2a,μm
1	0.060	0.60	0.20	138
2	0.070	0.66	0.38	132
3	0.065	0.65	0.61	135
4	0.070	0.64	0.95	133
5	0.064	1.40	0.20	125
6	0.066	1.41	0.36	124
7	0.073	1.44	0.62	120
8	0.063	1.38	0.93	126

The welds (6) were deposited using manual metal arc welding, the joint geometry being compatible with ISO-2560. Welding was carried out in the flat position using 4mm diameter electrodes and 20mm thickness base plate. The current and voltage used were 170A and 21V (DC+) respectively, the weld consisting of 27 runs with 3 beads per layer. The electrical energy input (Q) was stated as being approximately 1kJ/mm, the interpass temperature (T_i) being fixed at 200°C. Evans (14) has separately reported the time taken for his welds to cool over the temperature range 800-500°C, and this, together an analysis of the cooling curves for MMA welds (2) shows the cooling rate (dT/dt, °C/s) for this temperature range is well approximated by the equation:

$$dT/dt = [2155(T-T_i)^{1.6}]/[Q\eta] \qquad (12)$$

where η is the arc transfer efficiency, taken to be 0.775. Evans (6) did not report any grain size measurements, but analysis (2) of some of his other work (14-16) on Fe-Mn-Si-C welds suggests the following relationships, with a correlation coefficient of 0.95 (standard error 6.01):

$$\bar{L}_{tn}\ (\mu m) = 108.2 - 348C(wt.\%) - 9.6Mn(wt.\%) + 13.24Q(kJ/mm) \qquad (13)$$

The earlier experiments of Evans (14-16) do not include significant variations in Si concentration (0.27-0.41 wt.%), so that the above regression equation ignores Si as an independent variable; its inclusion would make the equation unreliable for Si values outside of the range of Evans' data. The excellent correlation coefficient obtained indicates this procedure to be satisfactory. Calculated grain size values using Eq. (13) are included in Table 1. Having established the necessary data, primary weld microstructures for welds 1-8 were calculated using the theory discussed earlier; the results are presented in Tables 2-3 and in Fig. 1. Bearing in mind that the cooling curves and grain sizes are estimated, agreement between theory and experiment is rather good. The correlation coefficient for a plot of the calculated versus experimental data (Fig. 1) is found to be 0.96. The mean experimental values of V_α, v_w and v_a are 0.23, 0.22 and 0.60 respectively, and the mean differences between calculated and experimental data are 0.05, 0.06, and 0.09 respectively. The good agreement confirms that the model (1) can be used satisfactorily to account for the relatively high Si concentrations used in Evans' experiments.

Table 2 - Calculated parameters for welds 1-8

Weld	q´,μm	t_1,s	t_2,s	G,μm/s	T_h-T_1,°C
1	10.7	3.61	0.211	218	804-600
2	9.0	3.31	0.211	147	800-610
3	10.0	3.41	0.211	177	808-610
4	9.5	3.51	0.211	151	816-610
5	7.1	2.64	0.211	79	735-600
6	7.0	2.68	0.211	72	738-600
7	6.5	2.71	0.211	59	740-600
8	7.7	2.77	0.211	105	760-610

Table 2 shows that for all the welds, $t_2=t_c$; the growth of Widmanstätten ferrite

is limited by hard impingement with intragranularly nucleated acicular ferrite. This is consistent with the micrographs published by Evans (6). When α_w is limited by impingement with α_a, v_w should depend to a large extent on G; this is indeed the case, the correlation coefficient relating them being 0.90.

Defining $\Delta=T_h-T_l$ (the temperature range over which α forms), Table 2 shows that Δ is slightly larger for weld 4 when compared with weld 1. In spite of this, t_l, q' and V_α are higher for weld 1. This is because ferrite formation begins at a higher temperature for weld 4 (T_h higher than weld 1) and since the cooling rate increases with T, there is less time available for α to grow. Experience from isotherml experiments would indicate that weld 4 should have a higher V_α (since its Si level is higher), and hence is misleading for the continuous cooling conditions that arise during welding. Keeping Δ constant but increasing T_h has the effect of reducing the amount of allotriomorphic ferrite. In such circumstances, Si should not influence toughness through microstructure, assuming that all else is constant.

On the other hand, if Si increases Δ, V_α should also increase. Comparison of welds 5 and 8 (which contain similar C, Mn and have similar grain size) illustrates this; q', t_l and V_α are all higher for the higher Si weld 8. In these circumstances Si should be detrimental to toughness.

Finally, it has already been pointed out that the experimental data (6) are not entirely suitable for the study of Si effects, since the other alloying additions have not been kept sufficiently constant. Indeed, precise control of weld composition is a major experimental difficulty. However, this is easy to do theoretically, and a major theoretical study of alloy effects on primary weld microstructure will be published later.

Table 3 - Comparison of calculated and experimental volume fractions of α, α_w and α_a. The superscripts 'c' and 'e' on the volume fractions indicate calculated and experimental data, respectively.

Weld	V_α^e	V_α^c	v_w^e	v_w^c	v_a^e	v_a^c
1	0.32	0.32	0.40	0.39	0.28	0.29
2	0.22	0.29	0.33	0.29	0.45	0.42
3	0.24	0.31	0.37	0.33	0.39	0.36
4	0.30	0.30	0.18	0.29	0.52	0.41
5	0.23	0.24	0.08	0.17	0.69	0.59
6	0.13	0.24	0.15	0.16	0.72	0.60
7	0.20	0.23	0.10	0.13	0.70	0.64
8	0.18	0.26	0.10	0.22	0.72	0.52

CONCLUSIONS

It has been demonstrated that a recent model for the prediction of the primary microstructure of low-alloy steel weld deposits (1-5) gives good agreement with published

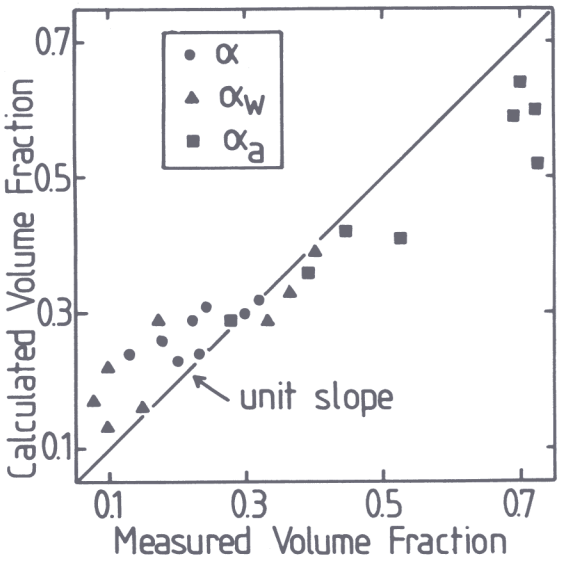

Fig. 1 - A plot of calculated α, α_w and α_a volume fractions versus the experimental data of Evans, for the weld deposits listed in Table 1.

experimental data (6) on the effect of large variations in Si and Mn on weld microstructure. The model predicts, and it is experimentally observed, that information obtained from simple isothermal experiments can be misleading in predicting alloying element effects.

ACKNOWLEDGEMENTS

The authors are grateful to Professor Hull for the provision of laboratory facilities at the University of Cambridge, and to ESAB AB (Sweden) for the provision of laboratory facilities and for financial support for this project.

REFERENCES

1) Bhadeshia, H. K. D. H., L. -E. Svensson and B. Gretoft, Acta Metall. 33 1271-1283 (1985).
2) Svensson, L.-E., B. Gretoft and H. K. D. H. Bhadeshia, Scand. J. of Metall. (1986) in press.
3) Gretoft, H. K. D. H. Bhadeshia and L.-E L.-E. Svensson, Acta Stereologica (1986) in press.
4) Bhadeshia, H. K. D. H., L.-E. Svensson and B. Gretoft, J. Mat. Sci. Let. 4 305-308 (1985).
5) Bhadeshia, H. K. D. H., L.-E. Svensson and B. Gretoft, Proc. 1st Int. Conf. on Computer Tech. in Welding, Welding Institute, Cambridge, England (1986), in press.
6) Evans, G. M., IIW document II-A-630-84 (1984).
7) Davies, G. J. and J. G. Garland, Int. Metall. Rev. 20 83-120 (1975).
8) Bhadeshia, H. K. D. H., L.-E. Svensson and B. Gretoft, J. Mat. Sci. (1986), in press.
9) Bhadeshia, H. K. D. H., Acta Metall. 29 1117-1130 (1981).

10) Bhadeshia, H. K. D. H., Met. Sci. 16 159-165 (1982).
11) Bhadeshia, H. K. D. H., Prog. in Mat. Sci. 29 321-386 (1985).
12) Bhadeshia, H. K. D. H., Mater. Sci. and Tech. 1 497-504 (1985).
13) Kinsman, K. R. and H. I. Aaronson, Metall. Trans. 4 959 (1973).
14) Evans, G. M., IIW document II-A-546-81.
15) Evans, G. M. IIW document II-A-469-79.
16) Evans, G. M., IIW document II-A-490-79.